https://doi.org/10.20965/ijat.2015.p0765

Paper:

Kinematics Analysis of a Novel 5-DOF Hybrid Manipulator

Wanjin Guo*,†, Ruifeng Li*, Chuqing Cao,***, and Yunfeng Gao***

*State Key Laboratory of Robotics and System, Harbin Institute of Technology
92 West Dazhi Street, Nan Gang District, Harbin 150001, China
E-mail: guowanjin0102@gmail.com
**School of Mechanical Engineering, Nanjing University of Science and Technology
Xiaolingwei 200, Nanjing 210094, China
***Wuhu HIT Robot Technology Research Institute Co., TLD.
E, Electronic Industrial Park, JiuJiang District, WuHu 241007, China
†Corresponding author

[Received June 2, 2015; accepted September 9, 2015]

Application of hybrid robotics is a continuously developing field, as hybrid manipulators have demonstrated that they can combine the benefits of serial structures and parallel mechanisms. In this paper, a novel 5-degree-of-freedom hybrid manipulator is designed. The structure of this manipulator and its kinematics analysis are presented. An innovative closed-form solution was proposed to address the inverse kinematics problem. Additionally, the validity of the closed-form solution was verified via co-simulation using MATLAB and ADAMS. Finally, the reachable workspace of this manipulator was obtained for further optimizing the structure and motion control.

Keywords: hybrid manipulator, kinematics, inverse kinematics, reachable workspace

1. Introduction

Hybrid robotic systems with advanced technology have been applied in various fields and have received more attention in recent years [1–5]. A hybrid manipulator combines the advantages of the serial mechanism (with a larger workspace) with those of the parallel mechanism (with a higher stiffness). Several 5-degree-of-freedom (DOF) hybrid manipulators have been investigated for applications, such as complex surface machining and robotic surgery. A synthesized mechanism, including 2 translational DOF and 1 rotational DOF (2T1R), was chosen as the parallel module of a 5-DOF hybrid machine tool [6, 7], which is capable of five-face machining in one setup. A 5-DOF hybrid machine, with a tool module on a 2T1R parallel manipulator and a rotary table, was proposed by Altuzarra et al. [8]. The resultant 3T2R motion pattern methodology was introduced to design machine typologies satisfying five-axis machining requirement. A 5-DOF hybrid manipulator, including a 3T1R parallel mechanism together with a single-axis rotational table, was developed to cut complex surfaces of soft materials [9]. However, the designs of these 5-DOF hybrid mechanisms mentioned above are quite complex, since a applications of a lower-mobility manipulator require a translation table [6, 7] or a rotary table [8, 9].

Several studies investigating 5-DOF hybrid manipulators with actuation redundancy or passive joint have been reported. A 5-DOF redundant hybrid machine tool, including a 3-DOF redundantly actuated parallel manipulator and a 2-DOF worktable, was presented by Wang et al. [10–12]. A lead screw and a guideway-slider subsystem were adopted to improve the stiffness of the machine tool. A 5-DOF hybrid-driven magnetic-resonance-compatible robot was designed for prostate brachytherapy [13]. A pair of slider-guide mechanisms with hybrid structure were adopted to perform translation and rotation motions. A 5-DOF hybrid parallel robot consisting of a 3-DOF positioning parallel module and a 2-DOF orientation serial module was proposed for a surgical laparoscope holder or for positioning and orientation of an active instrument [14]. In these configurations, the motion control of the hybrid machine tool [10–12] with actuation redundancy is more difficult than that for a non-redundant one. Similarly, it can be found in robots [13, 14] with passive joints.

Several other representative 5-DOF hybrid robots have been studied. Two 5-DOF machine tools, including a 3-DOF tripod and a 2-DOF spherical wrist, were introduced by Zoppi et al. [15]. A guideway-slider subsystem was adopted to improve the stiffness of the hybrid machine. A reconfigurable 5-DOF hybrid robot, which consists of a 2-DOF parallel spherical mechanism and a 3-DOF open-loop kinematic chain, was proposed by Liu et al. [16, 17]. Another 5-DOF reconfigurable hybrid robot, consisting of a 3-DOF parallel mechanism and a 2-DOF rotating head attached to a movable platform, was designed by Huang et al. [18]. However, all these 5-DOF hybrid robots [15, 16, 18] are required to perform in a relatively small workspace.

In the field of processing parts with freeform surfaces, a five-axis machine tool with hybrid architecture is a good solution. It is well known that hybrid machines can combine the benefits of the serial and parallel mechanisms

© Fuji Technology Press Ltd. Creative Commons CC BY-ND: This is an Open Access article distributed under the terms of the Creative Commons Attribution-NoDerivatives 4.0 International License (http://creativecommons.org/licenses/by-nd/4.0/).

while avoiding the drawbacks of either. The hybrid structure is helpful to enlarge the workspace and allow a flexible axis arrangement without introducing great complexity. Based on this motivation, this paper proposes a novel hybrid manipulator capable of five-face machining. The designed manipulator features good dexterity in orientation adjustment, positioning, and trajectory tracking control. In addition, an innovative closed-form solution is proposed to derive the inverse kinematics for this hybrid manipulator.

The remainder of this paper is organized as follows. The structure of the designed manipulator is analyzed in Section 2. The forward kinematics and the inverse kinematics of this manipulator are presented in Section 3. The validity of the proposed closed-form solution for the inverse kinematics is verified via numerical simulation and virtual prototype co-simulation in Section 4. The reachable workspace of this manipulator is determined in Section 5. Finally, conclusions are drawn in Section 6.

2. Configuration Description and Structure Analysis

The proposed 5-DOF manipulator configuration and drive system are described. Then, the main structure and its performance are analyzed.

2.1. Configuration Description

In order to achieve good dexterity in motion control of the designed manipulator, a hybrid design pattern is employed. The first two DOFs are achieved by a parallel mechanism, which provides good performance in terms of structural rigidity, and a simple configuration. The last three DOFs are achieved by a cantilever-like mechanism to satisfy the workspace requirement and the motion control performance. Although the rigidity of the overall structure of the hybrid manipulator will, to some extent, be affected by the cantilever-like mechanism, the objective of the designed manipulator with the capability of processing of complicated spatial surfaces and curves can be achieved by this hybrid design pattern.

The structure of this 5-DOF manipulator is shown in **Fig. 1**. It is a novel 3T2R hybrid manipulator, which consists of a 3-DOF (3T) parallel module and a 2-DOF (2R) serial module. Axes J_1, J_2, and J_3, consisting of ball screws, are driven by motors M_1, M_2, and M_3, respectively. Rotational axes J_4 and J_5 are driven by motors M_4 and M_5, respectively. Axis J_6 is taken as the end-effector, which is a high-speed motorized spindle. The nuts on screws S_1 and S_2 are fixedly connected to the slider assemblies A and C, respectively. Slider assembly B is rotated through a rotation shaft, which is connected to A, and slider assembly D is applied in the same way. Slider assemblies B and D are moved along the slide plate, which goes across S_1 and S_2. The turntable, which can rotate around axis J_t within a certain range, is fixed to the slide plate. In the meantime, the turntable moves the symmetry axis of S_1 and S_2 in the horizontal direction.

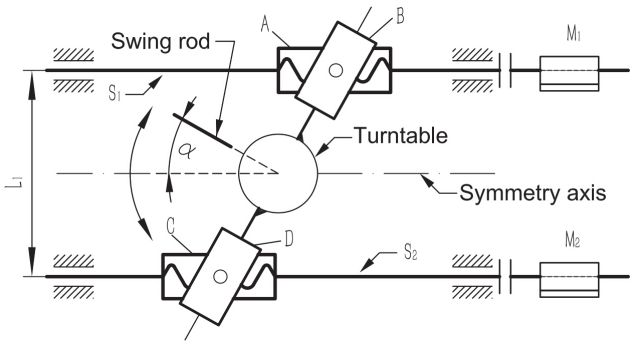

(a) Top view

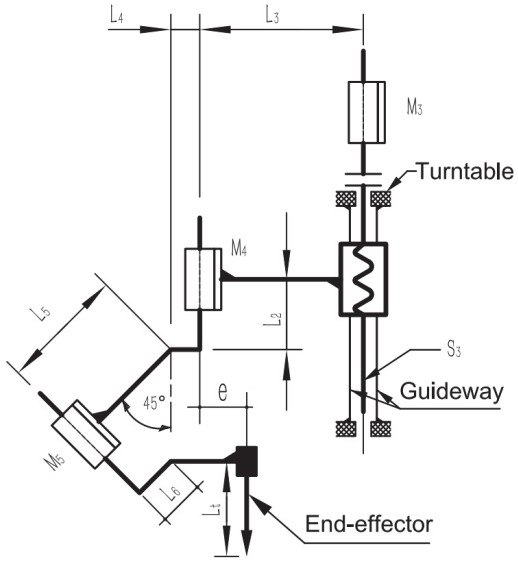

(b) Front view

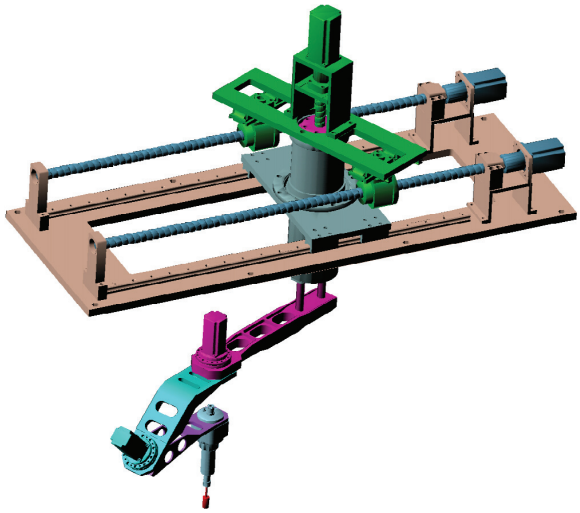

(c) 3D model

Fig. 1. Manipulator structure.

2.2. StructureAnalysis

The main structure of this 5-DOF manipulator consists of a parallel-driven component, a long straight rail component, a ball-screw-based linear drive component and serial mechanisms.

1) Parallel-driven component. The parallel-driven com-

ponent drives the manipulator translational movement in the horizontal plane. Compared to a typical serial manipulator, this drive mode can simplify the configuration, strengthen transmission stiffness, and reduce cost.

2) Long straight rail component. The long straight rail component with gantry mechanism features reduces the mass and gravity moments and inertia that transfers the majority of the gravity and overturn moments from the manipulator to the base framework. The performance of this component is superior to serial mechanisms, which must withstand the entire mass and gravity moments and inertia at the waist joint.

3) Ball-screw-based linear drive component. Compared to the general mechanism of a typical serial manipulator, the ball-screw-based linear drive reduces cost because it omits the relatively expensive reducer, and improves the efficiency and stiffness of the transmission system. Meanwhile, ball screws are easily integrated into linear axes. Compact actuator/drive packages are available, as well as components for custom integration.

4) Serial mechanisms. The serial mechanisms perform in series with the parallel mechanism and compensate for the defects of the parallel mechanism to satisfy the workspace requirement.

It is worth noting that the first two DOFs of the designed manipulator (i.e., the two translational movements in the horizontal plane) are achieved by a coupled mechanism. The movements are driven in parallel by M_1 and M_2 as shown in **Fig. 1**. Compared to the standard 2T design, this drive mode reduces cost and strengthens the transmission stiffness. The coupled mechanism simultaneously achieves two translational movements in the horizontal plane using two low-power motors, while the standard 2T design must translate in each direction using one high-power motor. Hence, the coupled mechanism reduces the cost of the motor and the reducer. Additionally, the coupled mechanism transfers the majority of the gravity and overturn moments from the manipulator to the base framework, while the standard 2T design generally utilizes a cross structure that only transfers the gravity and overturn moments to the base framework in one direction of translational movement.

Regarding the motion control of this manipulator, the orientation and the position of the end-effector are regulated by two rotation joints and three ball-screw drives, respectively. When the structure parameter e is equal to zero, decoupling-control of the orientation and the position of the end-effector can be achieved. In this case, the dexterity adjustment for the orientation of a certain processing point in the workspace can be achieved by changing only J_5, while the other axes can maintain stationary or vary only slightly. The movement of the end-effector can also be decoupled in the vertical direction and the horizontal plane. Hence, decoupling control of this manipulator structure can be implemented, i.e., the position and orientation of the end-effector can be independently planned for a trajectory. This process is equivalent to independently managing a 3-DOF mechanism and a 2-DOF mechanism for the inverse kinematics, motion planning, and other relevant issues, which allows the modeling and control for the task processing to be conveniently carried out. The major advantage of this manipulator is its ability to execute processing for complicated spatial surfaces and curves such as complex cavity molds and turbine blades.

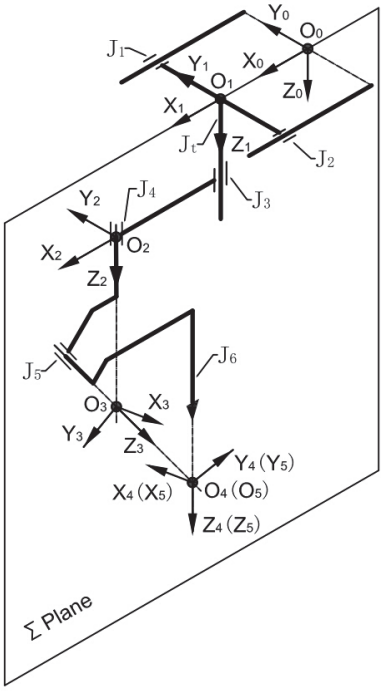

Fig. 2. Denavit-Hartenberg reference frame.

3. Kinematics Analysis

Based on the Denavit-Hartenberg method, the reference frames for this manipulator and the forward kinematics solution are presented. Then, a proposed algebraic method is applied to solve the inverse kinematics problem.

3.1. Forward Kinematics

The Denavit-Hartenberg method [19] was used to model the kinematics of this manipulator. The reference frames for this manipulator are assigned as shown in **Fig. 2**. The length of the rod i is denoted by L_i. The rotation angles of J_1, J_2, J_3, J_4, and J_5 are represented by φ_1, φ_2, φ_3, φ_4, and φ_5, respectively. The stroke of the nut along S_1, S_2, and S_3 are represented by X_1, X_2, and X_3, respectively. The distance between J_6 and J_4 in the horizontal direction is denoted as e. The rotation angle of J_t and link 1 is denoted as α. L_{01} represents the distance between point O_2 and point O_1 in the vertical direction

when the nut is located at the top starting point along S_3. These variables are related by

$$\alpha = \arctan\left((X_2 - X_1)/L_1\right) \quad . . . . . (1)$$

$$X_1 = s_x\varphi_1/(2\pi) \quad . . . . . (2)$$

$$X_2 = s_x\varphi_2/(2\pi) \quad . . . . . (3)$$

$$X_3 = s_z\varphi_3/(2\pi) \quad . . . . . (4)$$

where constant s_x represents the pitch of S_1 and S_2, and constant s_z represents the pitch of S_3.

Link 1 is driven in parallel by M_1 and M_2 as shown in **Figs. 1** and **2**. This link is moved along axis X_1, which is also the symmetry axis of S_1 and S_2. It is also rotated about J_t with the turntable when the stroke of A and C along the screw are different. Hence, a coupled movement is generated. The movement direction of link 1 along axis X_1 is always parallel to X_0 while this link is rotated about Z_1 and J_t. According to this movement relationship, the homogeneous transformation matrix ${}^0T_1$, which relates the spatial displacement of reference frame 1 to base reference frame 0, is directly given as

$${}^0T_1 = \begin{bmatrix} \cos\alpha & -\sin\alpha & 0 & (X_1+X_2)/2 \\ \sin\alpha & \cos\alpha & 0 & 0 \\ 0 & 0 & 1 & 0 \\ 0 & 0 & 0 & 1 \end{bmatrix} \quad . . (5)$$

The geometric parameters of this manipulator for links 2, 3, 4, and 5 (tool) shown in **Figs. 1** and **2** are listed in **Table 1**.

The homogeneous transformation matrix ${}^{i-1}T_i$ is constructed to provide a representation of reference frame i relative to reference frame $i-1$ according to the D-H reference frames and the geometric parameters. It is given as

$${}^{i-1}T_i = \begin{bmatrix} \cos\theta_i & -\cos\alpha_i\cdot\sin\theta_i & \sin\alpha_i\cdot\sin\theta_i & a_i\cdot\cos\theta_i \\ \sin\theta_i & \cos\alpha_i\cdot\cos\theta_i & -\sin\alpha_i\cdot\cos\theta_i & a_i\cdot\sin\theta_i \\ 0 & \sin\alpha_i & \cos\alpha_i & d_i \\ 0 & 0 & 0 & 1 \end{bmatrix} \quad . . . . . (6)$$

where $i = 2,\ldots,5, i \in N$.

By successive multiplications of the transformation matrices, the equivalent homogeneous transformation matrix ${}^0T_5$, which relates the spatial displacement of the tool frame to the base reference frame, is obtained as

$${}^0T_5 = {}^0T_1{}^1T_2{}^2T_3{}^3T_4{}^4T_5 = \begin{bmatrix} n_x & o_x & a_x & p_x \\ n_y & o_y & a_y & p_y \\ n_z & o_z & a_z & p_z \\ 0 & 0 & 0 & 1 \end{bmatrix}. \quad (7)$$

where

$$\vec{p} = [p_x, p_y, p_z]^T \quad . . . . . (8)$$

$$p_x = (X_1+X_2)/2 - e\cos(\alpha+\varphi_4) + L_3\cos\alpha \quad . (9)$$

$$p_y = L_3\sin\alpha - e\sin(\alpha+\varphi_4) \quad . . . . . (10)$$

$$p_z = L_2 + L_4 + \sqrt{2}L_5 + X_3 + L_{01} + e \quad . . . . (11)$$

Table 1. Geometric parameters of links.

Link i	θ_i	α_i	d_i	a_i
2	0	0	$X_3 + L_{01}$	L_3
3	$-\pi/2+\varphi_4$	$\pi/4$	$L_2+L_4+\sqrt{2}L_5$	0
4	$\pi+\varphi_5$	$\pi/4$	$\sqrt{2}e$	0
5	0	0	0	0

$$\vec{a} = [a_x, a_y, a_z]^T \quad . . . . . (12)$$

$$a_x = \cos(\alpha+\varphi_4)\frac{\cos\varphi_5 - 1}{2} - \frac{\sqrt{2}}{2}\sin(\alpha+\varphi_4)\sin\varphi_5 \quad . . . . . (13)$$

$$a_y = \sin(\alpha+\varphi_4)\frac{\cos\varphi_5 - 1}{2} + \frac{\sqrt{2}}{2}\cos(\alpha+\varphi_4)\sin\varphi_5 \quad . . . . . (14)$$

$$a_z = \frac{1+\cos\varphi_5}{2} \quad . . . . . (15)$$

$$\vec{o} = [o_x, o_y, o_z]^T \quad . . . . . (16)$$

$$o_x = \frac{\sqrt{2}}{2}\sin(\alpha+\varphi_4)\sin\varphi_5 - \cos(\alpha+\varphi_4)\frac{1+\cos\varphi_5}{2} \quad . . . . (17)$$

$$o_y = -\frac{\sqrt{2}}{2}\cos(\alpha+\varphi_4)\sin\varphi_5 0 - \sin(\alpha+\varphi_4)\frac{1+\cos\varphi_5}{2} \quad . . . . . (18)$$

$$o_z = \frac{1-\cos\varphi_5}{2} \quad . . . . . (19)$$

$$\vec{n} = [n_x, n_y, n_z]^T \quad . . . . . (20)$$

$$n_x = -\sin(\alpha+\varphi_4)\cos\varphi_5 - \frac{\sqrt{2}}{2}\cos(\alpha+\varphi_4)\sin\varphi_5 \quad . . . . . (21)$$

$$n_y = \cos(\alpha+\varphi_4)\cos\varphi_5 - \frac{\sqrt{2}}{2}\sin(\alpha+\varphi_4)\sin\varphi_5 \quad . . . . . (22)$$

$$n_z = -\frac{\sqrt{2}}{2}\sin\varphi_5 \quad . . . . . (23)$$

To verify the aforementioned forward kinematics solution, the concepts of the equivalent axis and the equivalent angle [20] are used to determine the spatial orientation that relates the representation of rotation from the tool reference frame to the base reference frame.

According to this manipulator structure configuration, the spatial orientation of the end-effector is determined by the rotations of J_t, J_4, and J_5. J_t and J_4 are both parallel

to Z_0. Hence, J_t and J_4 are represented as the equivalent unit vector axis $\vec{K}$. In this paper, the equivalent unit vector axes and the equivalent angles are represented as follows. J_t and J_4 are represented by $\vec{K}_1 = [0,0,1]^T$ and the equivalent angle $\theta_1 = \varphi_4 + \alpha$. J_5 is represented by the equivalent unit vector axis $\vec{K}_2 = \left[0, \sqrt{2}/2, \sqrt{2}/2\right]^T$ and the equivalent angle $\theta_2 = \varphi_5$. The rotation matrices are obtained as follows:

$$R\left(\vec{K}_1, \theta_1\right) = \begin{bmatrix} \cos\theta_1 & -\sin\theta_1 & 0 \\ \sin\theta_1 & \cos\theta_1 & 0 \\ 0 & 0 & 1 \end{bmatrix}, \quad \ldots\ldots (24)$$

$$R\left(\vec{K}_2, \theta_2\right) = \begin{bmatrix} \cos\theta_2 & -\frac{\sqrt{2}}{2}\sin\theta_2 & \frac{\sqrt{2}}{2}\sin\theta_2 \\ \frac{\sqrt{2}}{2}\sin\theta_2 & \frac{1+\cos\theta_2}{2} & \frac{1-\cos\theta_2}{2} \\ -\frac{\sqrt{2}}{2}\sin\theta_2 & \frac{1-\cos\theta_2}{2} & \frac{1+\cos\theta_2}{2} \end{bmatrix}. \quad \ldots\ldots\ldots\ldots (25)$$

As shown in **Fig. 2**, the initial orientation, which relates the tool reference frame to the base reference frame, is expressed as

$${}^0R_5^{IS} = \begin{bmatrix} 0 & -1 & 0 \\ 1 & 0 & 0 \\ 0 & 0 & 1 \end{bmatrix} \ldots\ldots\ldots\ldots (26)$$

The spatial orientation ${}^0R_5$, which relates the orientation transformation of the tool reference frame to the base reference frame, is obtained by successive multiplication of the rotation matrices. It is given as

$$\begin{aligned} {}^0R_5 &= {}^0R_5^{IS} \cdot R\left(\vec{K}_1, \theta_1\right) \cdot R\left(\vec{K}_2, \theta_2\right) \\ &= \left[\vec{u} \;\; \vec{v} \;\; \vec{w}\right] \quad \ldots\ldots\ldots (27) \end{aligned}$$

where $\theta_1 = \varphi_4 + \alpha$, $\theta_2 = \varphi_5$, and the detailed vectors are expressed as

$$\vec{u} = \begin{bmatrix} -\sin\theta_1\cos\theta_2 - \frac{\sqrt{2}}{2}\cos\theta_1\sin\theta_2 \\ \cos\theta_1\cos\theta_2 - \frac{\sqrt{2}}{2}\sin\theta_1\sin\theta_2 \\ -\frac{\sqrt{2}}{2}\sin\theta_2 \end{bmatrix}, \quad \ldots (28)$$

$$\vec{v} = \begin{bmatrix} \frac{\sqrt{2}}{2}\sin\theta_1\sin\theta_2 - \cos\theta_1\frac{1+\cos\theta_2}{2} \\ -\frac{\sqrt{2}}{2}\cos\theta_1\sin\theta_2 - \sin\theta_1\frac{1+\cos\theta_2}{2} \\ \frac{1-\cos\theta_2}{2} \end{bmatrix}, \quad (29)$$

$$\vec{w} = \begin{bmatrix} \cos\theta_1\frac{\cos\theta_2 - 1}{2} - \frac{\sqrt{2}}{2}\sin\theta_1\sin\theta_2 \\ \sin\theta_1\frac{\cos\theta_2 - 1}{2} + \frac{\sqrt{2}}{2}\cos\theta_1\sin\theta_2 \\ \frac{1+\cos\theta_2}{2} \end{bmatrix}. \quad \ldots (30)$$

As shown in Eqs. (12), (16), (20), (28), (29), and (30), the expressions for $\vec{u}$, $\vec{v}$, and $\vec{w}$ are identical to the ones for $\vec{n}$, $\vec{o}$ and $\vec{a}$, respectively. Hence, the orientation validity of the forward kinematics solution is confirmed.

3.2. The Proposed Closed-Form Solution for Inverse Kinematics

The inverse kinematics problem of a manipulator is to find the values of the joint positions given the position and orientation of the end-effector relative to the base and the values of all of the geometric link parameters. The disadvantages of numerical methods are that they can be slower and in some cases, they do not allow computation of all possible solutions. Therefore, closed-form solutions are desirable because they are faster than numerical solutions and readily identify all possible solutions. Since the structure of this 5-DOF manipulator satisfies the Pieper criterion [21], an algebraic method is applied to solve the inverse kinematics problem. Based on the particular geometric features of this manipulator, only the orientation vector $\vec{a}$ and the position vector $\vec{p}$ are selected to propose an innovative closed-form solution for the inverse kinematics.

3.2.1. Orientation Vector Selection

In order to select one or several vectors from the spatial orientation of the forward kinematics for the inverse kinematics, the equivalent unit vector must be found to represent the end-effector in the base reference frame.

The unit vector of the end-effector is denoted by $\vec{K}_e = [0,0,1]^T$ in the tool reference frame. Rotating J_5, J_4, and J_t, the unit vector $\vec{K}$ that relates the orientation transformation of the tool reference frame to the base reference frame is represented as

$$\begin{aligned} \vec{K} &= {}^0R_5^{IS} \cdot R\left(\vec{K}_1, \theta_1\right) \cdot R\left(\vec{K}_2, \theta_2\right) \cdot \vec{K}_e \\ &= \begin{bmatrix} \cos\theta_1\frac{\cos\theta_2 - 1}{2} - \frac{\sqrt{2}}{2}\sin\theta_1\sin\theta_2 \\ \sin\theta_1\frac{\cos\theta_2 - 1}{2} + \frac{\sqrt{2}}{2}\cos\theta_1\sin\theta_2 \\ \frac{1+\cos\theta_2}{2} \end{bmatrix} \quad (31) \end{aligned}$$

where $R\left(\vec{K}_1, \theta_1\right)$ and $R\left(\vec{K}_2, \theta_2\right)$ are given by Eqs. (24) and (25), respectively.

As shown in Eqs. (12) and (31), $\vec{a}$ and $\vec{K}$ have the same expression. Therefore, $\vec{a}$ is selected from the spatial ori-

entation for solving the inverse kinematics, which satisfies the orientation requirement.

3.2.2. The Detailed Closed-Form Solution

The proposed closed-form solution for the inverse kinematics and its concise expressions are derived as follows.

Step 1. Solving φ_5.

Eq. (15) is rewritten as

$$\cos\varphi_5 = 2a_z - 1 \quad \ldots\ldots\ldots\ldots\ldots\ldots (32)$$

Based on Eq. (32), φ_5 is obtained as

$$\varphi_5 = \arccos(2a_z - 1) \quad \ldots\ldots\ldots\ldots\ldots\ldots (33)$$

or

$$\varphi_5 = -\arccos(2a_z - 1) \quad \ldots\ldots\ldots\ldots\ldots\ldots (34)$$

Step 2. Solving φ_4.

A new variable is defined as

$$\theta = \alpha + \varphi_4. \quad \ldots\ldots\ldots\ldots\ldots\ldots (35)$$

Substituting Eq. (35) into Eqs. (13) and (14) yields

$$\sin\theta = -\frac{2\sqrt{2}a_x\sin\varphi_5 + 2a_y(1-\cos\varphi_5)}{2\sin^2\varphi_5 + (1-\cos\varphi_5)^2} \quad \ldots (36)$$

and

$$\cos\theta = -\frac{2a_x(1-\cos\varphi_5) - 2\sqrt{2}a_y\sin\varphi_5}{2\sin^2\varphi_5 + (1-\cos\varphi_5)^2}. \quad \ldots (37)$$

An equation is then obtained as

$$\tan\theta = \frac{-\left(\sqrt{2}a_x\sin\varphi_5 + a_y(1-\cos\varphi_5)\right)}{-\left(a_x(1-\cos\varphi_5) - \sqrt{2}a_y\sin\varphi_5\right)}. \quad \ldots (38)$$

Based on Eq. (32), the following equations are obtained

$$\sin\varphi_5 = 2\sqrt{a_z - a_z^2} \quad \ldots\ldots\ldots\ldots\ldots\ldots (39)$$

or

$$\sin\varphi_5 = -2\sqrt{a_z - a_z^2}. \quad \ldots\ldots\ldots\ldots\ldots\ldots (40)$$

According to Eq. (1), giving

$$\sin\alpha = (e\sin\theta + p_y)/L_3. \quad \ldots\ldots\ldots\ldots\ldots\ldots (41)$$

There are two cases according to the different possible values for $\sin\varphi_5$.

Case 1: $\sin\varphi_5 = 2\sqrt{a_z - a_z^2}$.

Substituting Eqs. (32) and (39) into Eq. (38) yields

$$\theta_1 = \arctan 2\left(-\left(\sqrt{2}a_x\sqrt{a_z - a_z^2} + a_y(1-a_z)\right), -\left(a_x(1-a_z) - \sqrt{2}a_y\sqrt{a_z - a_z^2}\right)\right) \quad \ldots (42)$$

Substituting Eq. (42) into Eq. (41) yields

$$\alpha_1 = \arcsin\left((e\sin\theta_1 + p_y)/L_3\right) \quad \ldots\ldots\ldots\ldots (43)$$

According to Eqs. (35), (42) and (43), φ_4 is given as

$$\varphi_4 = \theta_1 - \alpha_1 \quad \ldots\ldots\ldots\ldots\ldots\ldots (44)$$

Case 2: $\sin\varphi_5 = -2\sqrt{a_z - a_z^2}$.

Substituting Eqs. (32) and (40) into Eq. (38) yields

$$\theta_2 = \arctan 2\left(-\left(-\sqrt{2}a_x\sqrt{a_z - a_z^2} + a_y(1-a_z)\right), -\left(a_x(1-a_z) + \sqrt{2}a_y\sqrt{a_z - a_z^2}\right)\right) \quad \ldots (45)$$

Substituting Eq. (45) into Eq. (41) yields

$$\alpha_2 = \arcsin\left((e\sin\theta_2 + p_y)/L_3\right) \quad \ldots\ldots\ldots\ldots (46)$$

According to Eqs. (35), (45), and (46), φ_4 is obtained as

$$\varphi_4 = \theta_2 - \alpha_2 \quad \ldots\ldots\ldots\ldots\ldots\ldots (47)$$

Step 3. Solving $\mathbf{X_1(\varphi_2)}$ and $\mathbf{X_2(\varphi_2)}$.

According to Eq. (1), giving

$$\tan\alpha = (X_2 - X_1)/L_1 \quad \ldots\ldots\ldots\ldots\ldots\ldots (48)$$

Combining Eqs. (9) and (48) leads to

$$\begin{cases} X_2 - X_1 = L_1\tan\alpha \\ X_1 + X_2 = 2(p_x + e\cos\theta - L_3\cos\alpha) \end{cases} \quad \ldots (49)$$

According to Eq. (49), $X_1(\varphi_1)$ and $X_2(\varphi_2)$ are expressed as

$$X_1 = p_x + e\cos\theta - L_3\cos\alpha - (L_1\tan\alpha)/2 \quad \ldots (50)$$

$$\varphi_1 = 2\pi X_1/s_x \quad \ldots\ldots\ldots\ldots\ldots\ldots (51)$$

and

$$X_2 = p_x + e\cos\theta - L_3\cos\alpha + (L_1\tan\alpha)/2 \quad \ldots (52)$$

$$\varphi_2 = 2\pi X_2/s_x \quad \ldots\ldots\ldots\ldots\ldots\ldots (53)$$

The results of $X_1(\varphi_1)$ and $X_2(\varphi_2)$ are obtained by substituting the group of θ_1 and α_1 (or the group of θ_2 and α_2) into the above equations.

Step 4. Solving $\mathbf{X_3(\varphi_3)}$.

According to Eqs. (11), X_3 and φ_3 are expressed as

$$X_3 = p_z - \left(L_2 + L_4 + \sqrt{2}L_5\right) - L_{01} - e \quad \ldots (54)$$

$$\varphi_3 = 2\pi X_3/s_z \quad \ldots\ldots\ldots\ldots\ldots\ldots (55)$$

4. Kinematics Simulation

The proposed closed-form solution for the inverse kinematics is verified by simulating the kinematics with the assumed structure parameters (**Table 2**) based on MATLAB and ADAMS.

A saddle surface is chosen in the kinematics simulation for the grinding task of this manipulator. In this paper, the

Table 2. The assumed manipulator structure parameters (mm).

L_1	L_2	L_3	L_4	L_5	L_6	e	Lt	$L01$	s_x	s_z
420	50	450	180	180	80	30	285	400	10	10

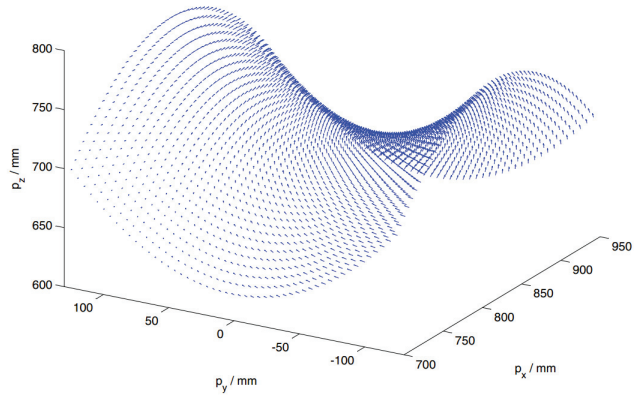

(a) Desired trajectory

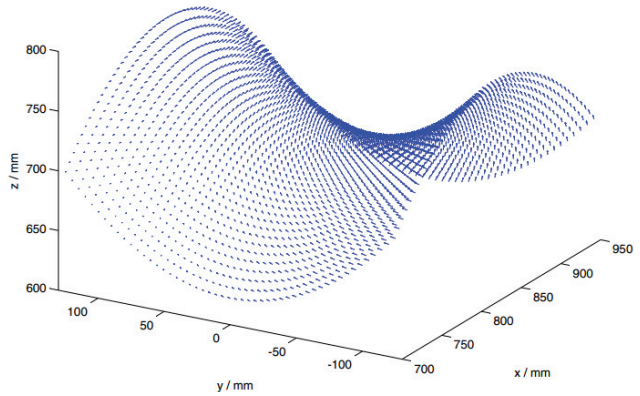

(b) Traversed trajectory

Fig. 3. Saddle surface trajectory.

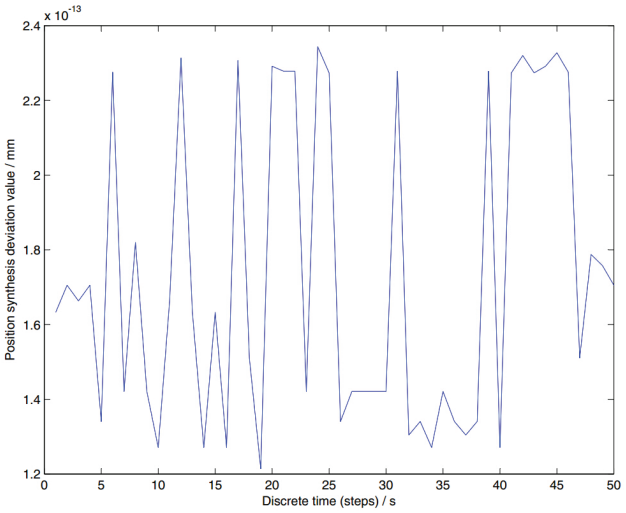

(a) Position synthesis deviation

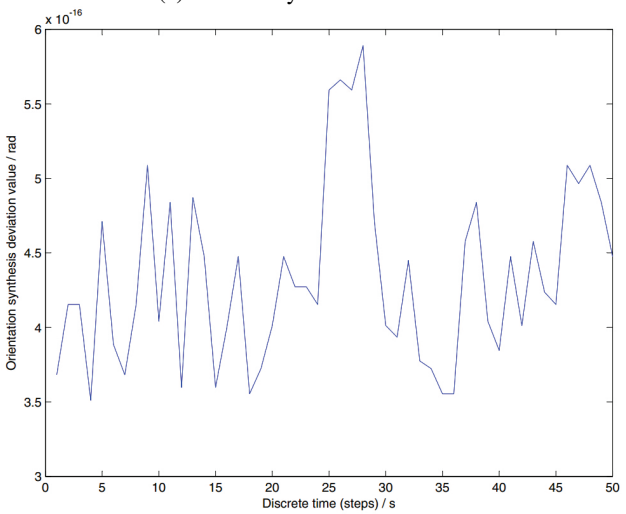

(b) Orientation synthesis

Fig. 4. Synthesis deviation.

equation of the saddle surface is expressed as

$$z = -\left[(x-825)^2/200 - y^2/200\right] + 700. \quad \ldots (56)$$

The function of the tool trajectory is given as

$$\begin{cases} x = 700 + 5t \\ y = -125 + 5t \\ z = -\left[(x-825)^2/200 - y^2/200\right] + 700 \end{cases}$$
$$t \in [0,\ 50] \quad \ldots (57)$$

4.1. MATLAB Numerical Simulation

The discrete positions $(p_x, p_y, p_z)^T$ and discrete orientations $(a_x, a_y, a_z)^T$ of the desired tool trajectory are calculated by the given saddle equation (Eq. (56)) and the trajectory function (Eq. (57)). The desired saddle surface is drawn as shown in **Fig. 3(a)**, where the orientation equals the unit normal vector of the corresponding discrete position and points at the corresponding discrete position.

The joint angles φ_1, φ_2, φ_3, φ_4, and φ_5 are obtained via MATLAB simulation based on the proposed closed-form solution and the desired tool trajectory ($(p_x, p_y, p_z)^T$ and $(a_x, a_y, a_z)^T$). According to these joint angles, the position $(x, y, z)^T$ and orientation $(u, v, w)^T$ of the tool traversal trajectory are calculated based on the forward kinematics. The traversed saddle surface is drawn as shown in **Fig. 3(b)**.

According to this simulation, the position and orientation of the desired trajectory are achieved. Details of the traversed trajectory are also obtained. The position synthesis deviation Δd and the orientation synthesis deviation $\Delta\delta$ are defined as

$$\Delta d = \sqrt{(p_x - x)^2 + (p_y - y)^2 + (p_z - z)^2}, \quad \ldots (58)$$

$$\Delta\delta = \sqrt{(a_x - u)^2 + (a_y - v)^2 + (a_z - w)^2}. \quad \ldots (59)$$

These synthesis deviations are calculated, as shown in **Fig. 4**. The maximum values are given as

$$\Delta d_{\max} = 2.3437 \times 10^{-13} \quad \text{mm}, \quad \ldots (60)$$

$$\Delta\delta_{\max} = 5.8915 \times 10^{-16} \quad \text{rad}. \quad \ldots (61)$$

Comparing the desired tool trajectory (which is cal-

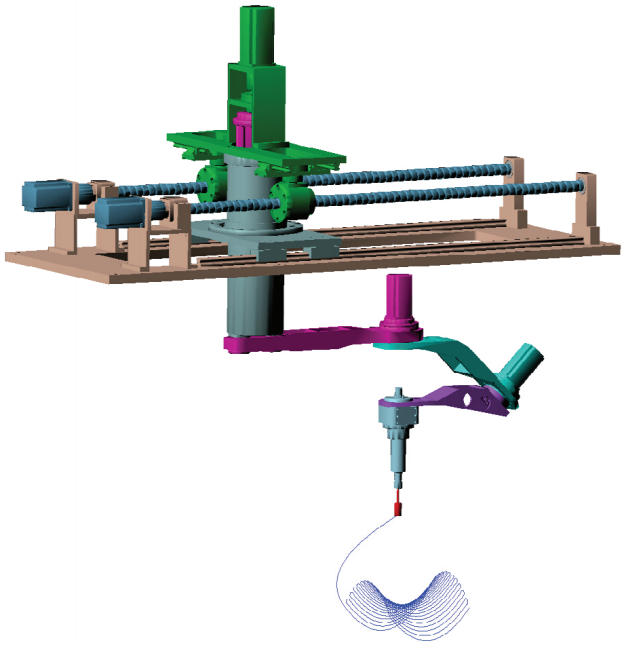

Fig. 5. The simulation of the virtual prototype model.

culated by the given saddle equation and the trajectory function) and the tool traversal trajectory (which is obtained based on the discrete desired trajectory, the proposed closed-form solution and the forward kinematics), the position and orientation synthesis deviations are all extremely small. More details can be found in **Fig. 4**. Hence, the proposed closed-form solution for inverse kinematics is valid and effective.

4.2. Virtual Prototype Co-Simulation

In order to illustrate this manipulator movement and validate the proposed closed-form solution, a virtual prototype technology is introduced for kinematics co-simulation in ADAMS and MATLAB. The process and results are outlined as follows.

The virtual prototype model was developed in ADAMS/View based on the geometric structure of the designed manipulator generated by SOLIDWORKS. The joint motions were obtained corresponding to the joint angles (φ_1, φ_2, φ_3, φ_4, and φ_5) using the proposed closed-form solution of the inverse kinematics in a MATLAB simulation. An interactive control kinematics simulation was conducted for the saddle surface grinding task of this manipulator. The simulation of the virtual prototype model is shown in **Fig. 5**. The movements of tool and other components are dexterous, smooth, and continuous, without uneven variation or any mutual interference in the entire virtual simulation process.

Comparing the trajectory for the tool's spatial displacement (i.e., the traversed saddle surface) in ADAMS the desired tool trajectory (i.e., the desired saddle surface) in MATLAB, a desirable match was observed, with magnitudes of the synthesis deviations within 10^{-10}. This illustrates the overall consistency of the orientations, because

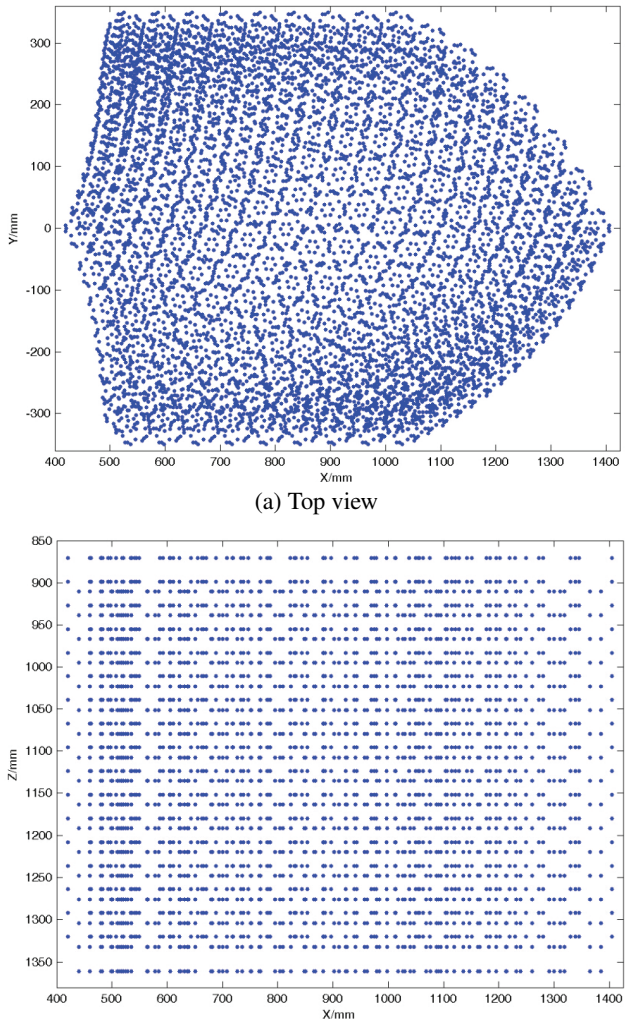

(a) Top view

(b) Front view

Fig. 6. Manipulator workspace.

the orientations of the desired tool trajectory are determined by the discrete positions of the desired trajectory. The validity and feasibility of the proposed closed-form solution for the inverse kinematics have thus been verified.

5. Manipulator Workspace

The reachable workspace [22] of this manipulator was obtained through MATLAB simulation based on the forward kinematics solution with the assumed parameters of the structure (**Table 2**). The reachable workspace of this manipulator is shown in **Fig. 6**.

In the top view of the **Fig. 6**, the shapes of the left end and the right end are different, which is caused by the sway of the swing rod. The sway values are $L_3 \cos\alpha$ and $L_3 \sin\alpha$ in the X and Y directions, respectively. In the start phase, α increases from zero to the maximum attainable value, and the sway value in the X and Y directions gradually decrease and increase, respectively. In the end phase, α decreases from the maximum attainable value

to zero, and the sway values in the X and Y directions gradually increase and decrease, respectively. The mutual variation relationship is shown in **Fig. 6(a)**. The range in the Z direction of this manipulator workspace is shown in **Fig. 6(b)**. The top view and the front view of **Fig. 6** show the range in the X, Y, and Z direction of the reachable workspace.

6. Conclusions

A novel 5-DOF hybrid manipulator with five-face machining capability is proposed. The characteristics of the proposed manipulator for complex surface machining are demonstrated based on simulations. Additionally, the inverse kinematics problem of this manipulator was solved to obtain a closed-form solution. To summarize, the major contributions of this paper are as follows.

(1) A novel 5-DOF hybrid manipulator was designed and analyzed. The manipulator has good dexterity in orientation adjustment and trajectory tracking based on the specific qualities. The reachable workspace of the manipulator was obtained for further optimizing the structure and the motion control.

(2) An innovative closed-form solution was developed to address the inverse kinematics problem for this 5-DOF hybrid manipulator and other similar structures.

(3) The closed-form solution of the inverse kinematics was verified by numerical simulation and co-simulation of a virtual prototype. Meanwhile, the kinematic and dexterous characteristics were tested by machining a complex surface in the co-simulation.

In future work, the structure optimization, dynamics problem, and motion control will be further considered. Furthermore, the manipulator will be integrated with a vision system to study workpiece reconstruction strategies.

Acknowledgements

This work was supported by the National High-tech R&D Program (863 Program) of China (No. 2013AA040902-2).

References:

[1] M. Okada, H. Kozuka, H. Tachiya, T. Iwasaki, and Y. Yamashita, "Burnishing Process Using Spherical 5-DOF Hybrid-Type Parallel Mechanism with Force Control," Int. J. of Automation Technology, Vol.8, pp. 243-252, 2014.

[2] B. Denkena and F. Flöter, "Adaptive Cutting Force Control with a Hybrid Axis System," Int. J. of Automation Technology, Vol.7, pp. 378-384, 2013.

[3] Y.-T. Liu, H.-L. Wu, J.-Y. Wang, and Y. Yamagata, "Contact-Type Profile Measuring Device Using Laser Interferometry System Incorporating Hybrid Actuating System," Int. J. of Automation Technology, Vol.7, pp. 489-497, 2013.

[4] D. Pisla, A. Szilaghyi, C. Vaida, and N. Plitea, "Kinematics and workspace modeling of a new hybrid robot used in minimally invasive surgery," Robotics and Computer-Integrated Manufacturing, Vol.29, pp. 463-474, 2013.

[5] P. Ben-Tzvi, "Experimental validation and field performance metrics of a hybrid mobile robot mechanism," Journal of Field Robotics, Vol.27, pp. 250-267, 2013.

[6] F. Xie, X.J. Liu, Z. You, and J. Wang, "Type synthesis of 2T1R-type parallel kinematic mechanisms and the application in manufacturing," Robotics and Computer-Integrated Manufacturing, Vol.30, pp. 1-10, 2014.

[7] F. Xie, X.J. Liu, and T. Li, "Type Synthesis and Typical Application of 1T2R-Type Parallel Robotic Mechanisms," Mathematical Problems in Engineering, Vol.2013, pp. 1-12, 2013.

[8] O. Altuzarra, Y. S. Martín, E. Amezua, and A. Hernández, "Motion pattern analysis of parallel kinematic machines: A case study," Robotics and Computer-Integrated Manufacturing, Vol.25, pp. 432-440, 2009.

[9] V. Sangveraphunsiri and K. Chooprasird, "Dynamics and control of a 5-DOF manipulator based on an H-4 parallel mechanism," The International Journal of Advanced Manufacturing Technology, Vol.52, pp. 343-364, 2010.

[10] L. Wang, J. Wu, J. Wang, and Z. You, "An experimental study of a redundantly actuated parallel manipulator for a 5-DOF hybrid machine tool," Mechatronics, IEEE/ASME Transactions on, Vol.14, pp. 72-81, 2009.

[11] J. Wu, J. Wang, L. Wang, T. Li, and Z. You, "Study on the stiffness of a 5-DOF hybrid machine tool with actuation redundancy," Mechanism and Machine Theory, Vol.44, pp. 289-305, 2009.

[12] J. Wu, J. Wang, L. Wang, and T. Li, "Dynamic model and force control of the redundantly actuated parallel manipulator of a 5-DOF hybrid machine tool," Robotica, Vol.27, pp. 59-65, 2008.

[13] S. Jiang, J. Guo, S. Liu, J. Liu, and J. Yang, "Kinematic analysis of a 5-DOF hybrid-driven MR compatible robot for minimally invasive prostatic interventions," Robotica, Vol.30, pp. 1147-1156, 2012.

[14] B. Gherman, D. Pisla, C. Vaida, and N. Plitea, "Development of inverse dynamic model for a surgical hybrid parallel robot with equivalent lumped masses," Robotics and Computer-Integrated Manufacturing, Vol.28, pp. 402-415, 2012.

[15] M. Zoppi, D. Zlatanov, and R. Molfino, "Kinematics analysis of the Exechon tripod," ASME 2010 International Design Engineering Technical Conferences and Computers and Information in Engineering Conference, American Society of Mechanical Engineers, pp. 1381-1388, 2010.

[16] H. Liu, J. Mei, X. Zhao, T. Huang, and D. G. Chetwynd, "Inverse dynamics and servomotor parameter estimation of a 2-DOF spherical parallel mechanism," Science in China Series E: Technological Sciences, Vol.51, pp. 288-301, 2008.

[17] H. Liu, T. Huang, J. Mei, X. Zhao, D. G. Chetwynd, M. Li, and S. Jack Hu, "Kinematic Design of a 5-DOF Hybrid Robot with Large Workspace/Limb-Stroke Ratio," Journal of Mechanical Design, Vol.129, pp. 530-537, 2007.

[18] T. Huang, M. Li, X. Zhao, J. Mei, D. G. Chetwynd, and S. J. Hu, "Conceptual design and dimensional synthesis for a 3-DOF module of the TriVariant-a novel 5-DOF reconfigurable hybrid robot," Robotics, IEEE Transactions on, Vol.21, pp. 449-456, 2005.

[19] J. Denavit, "A kinematic notation for lower-pair mechanisms based on matrices," Trans. of the ASME. Journal of Applied Mechanics, Vol.22, pp. 215-221, 1955.

[20] B. Siciliano and O. Khatib, "Springer handbook of robotics," Springer, 2008.

[21] D. L. Peiper, "The kinematics of manipulators under computer control," DTIC Document, 1968.

[22] B. Roth, "Performance evaluation of manipulators from a kinematic viewpoint," NBS Special Publication, Vol.459, pp. 39-62, 1976.

Name:
Wanjin Guo

Affiliation:
Ph.D Candidate, State Key Laboratory of Robotics and System, Harbin Institute of Technology (HIT)

Address:
92 West Dazhi Street, Nan Gang District, Harbin, China

Brief Biographical History:
2007- Bachelor of Engineering at School of Construction Machinery, Chang'an University
2010- Master of Engineering at School of Electro-Mechanical Engineering, Xidian University
2012- Ph.D student, State Key Laboratory of Robotics and System, Harbin Institute of Technology (HIT)

Name:
Ruifeng Li

Affiliation:
Professor, State Key Laboratory of Robotics and System, Harbin Institute of Technology (HIT)
Deputy Director, State Key Laboratory of Robotics and System, Harbin Institute of Technology (HIT)

Address:
92 West Dazhi Street, Nan Gang District, Harbin, China

Brief Biographical History:
1997- Doctorate of Engineering at School of Mechatronics Engineering, Harbin Institute of Technology
2004- Professor, State Key Laboratory of Robotics and System, Harbin Institute of Technology
2007- Ph.D Supervisor, State Key Laboratory of Robotics and System, Harbin Institute of Technology

Main Works:
- "Feature Representation for Facial Expression Recognition Based on FACS and LBP," International Journal of Automation and Computing, Vol.11, pp. 459-468, Otc. 2014.
- "A Novel Automatic Facial Expression Recognition Method Based on AAM," Journal of Computers, Vol.9, pp. 608-617, Mar. 2014.
- "On-Line Identification of Line Segments Using Hypothesis Testing for Robot Mapping," Advanced Materials Research, Vol.902, pp. 245-249, Feb. 2014.
- "Efficient Feature Representation for Human Action Recognition in DS&SP," Advanced Materials Research, Vols.889-890, pp. 1057-1064, Feb. 2014.

Membership in Academic Societies:
- Robotics Association of Heilongjiang Province, Chairman
- Intelligent Robot Professional Committee of Chinese Association for Artificial Intelligence, Permanent Member
- Robot Professional Committee of Chinese Association of Automation, Member
- Industrial Robot Sub-Committee of China Association for Standardization, Member
- Robot Professional Committee of Chinese Society of Astronautics, Member

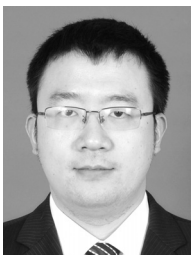

Name:
Chuqing Cao

Affiliation:
Assistant Professor, School of Mechanical Engineering, Nanjing University of Science and Technology

Address:
Xiaolingwei 200, Nanjing, China

Brief Biographical History:
2012- Doctorate of Engineering at School of Mechatronics Engineering, Harbin Institute of Technology
2014- Assistant Professor, School of Mechanical Engineering, Nanjing University of Science and Technology

Main Works:
- "Hand posture recognition via joint feature sparse representation," Optical Engineering, Vol.50, pp. 127210-1-127210-10, Dec. 2011.

Name:
Yunfeng Gao

Affiliation:
Associate Professor, State Key Laboratory of Robotics and System, Harbin Institute of Technology (HIT)

Address:
92 West Dazhi Street, Nan Gang District, Harbin, China

Brief Biographical History:
1991- Master of Engineering at School of Mechatronics Engineering, Harbin Institute of Technology
2000- Associate Professor, Key Laboratory of Robot and System, Harbin Institute of Technology

Main Works:
- "Video System design of a miniature cable-free robot for LESS," Mechatronics and Automation (ICMA 2014), Tianjin, China, pp. 535-540, Aug. 2014.
- "Connected Components Labeling Algorithm Based On Run-length Table Searching," The 9th International Conference onComputer Science & Education (ICCSE 2014), Vancouver, Canada, pp. 700-704, Aug. 2014.
- "Positioning Approach for Indoor Autonomous Mobile Robot Using a Single Ultrasonic Sensor Pair," Information and Automation (ICIA 2013), Yinchuan, China, pp. 787-792, Aug. 2013.
- "Research Overview of Indoor Localization Methods for Autonomous Mobile Robots," Transducer and Microsystem Technologies, Vol.32, pp. 1-5, 2013.

Membership in Academic Societies:
- Institute of Electrical and Electronics Engineers (IEEE), Member
- Robot Professional Committee of Chinese Society of Astronautics, Member